Faraday Discussions

Accepted Manuscript

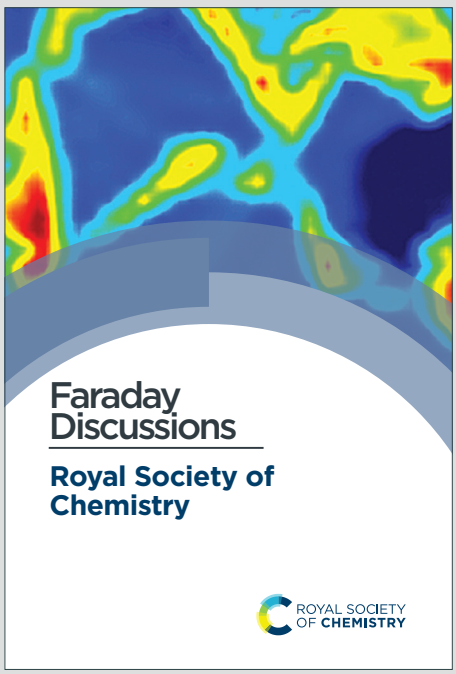

This article can be cited before page numbers have been issued, to do this please use: A. Ismail, J. Yang, S. Kalluvadiveetil, L. Maduro, H. Jyothilal, R. Dryfe, A. Keerthi and R. Boya, *Faraday Discuss.*, 2026, DOI: 10.1039/D5FD00142K.

ROYAL SOCIETY OF CHEMISTRY

www.rsc.org/faraday_d

When does nanofluidic memory disappear? Understanding and reinstating memristive behavior of ionic liquids in two-dimensional nanochannels

View Article Online
DOI: 10.1039/D5FD00142K

Abdulghani Ismail[1,2,3¥] , Jing Yang[4,5¥], Kalluvadi Veetil Saurav[2,4], Louis Maduro[1,2], Hiran Jyothilal[1,2], Robert A. W. Dryfe[4,5], Ashok Keerthi[2,4,6], Boya Radha[1,2,6*]

[1] Department of Physics and Astronomy, School of Natural Sciences, The University of Manchester, Manchester M13 9PL, United Kingdom

[2] National Graphene Institute, The University of Manchester, Manchester M13 9PL, United Kingdom

[3] Univ. Paris-Saclay, CNRS, Institut Galien Paris-Saclay, Orsay 91400, France

[4] Department of Chemistry, School of Natural Sciences, The University of Manchester, Manchester M13 9PL, United Kingdom

[5] Henry Royce Institute, University of Manchester, Manchester, M13 9PL, United Kingdom

[6] Photon Science Institute, The University of Manchester, Manchester M13 9PL, United Kingdom

[¥] These authors equally contributed

*Correspondence to be addressed to: radha.boya@manchester.ac.uk

Abstract

Nanofluidic memristors rely on ionic transport in confined nanochannels that depends on the history of the applied voltage, producing pinched hysteresis loops. Yet the conditions under which this memory emerges or disappears remain poorly understood. Here, we investigate the role of the solvent in tuning ion-ion correlations and assess the necessity of asymmetric boundary conditions for generating memristive behavior in ångström-scale two-dimensional (2D) nanochannels. With this nanochannel platform, previously shown to yield four distinct loop styles with aqueous electrolytes, we replace water with room-temperature ionic liquids (RTILs) and RTIL/solvent mixtures. Pure EMIM-TFSI exhibits only non-pinched capacitive I-V loops, demonstrating that extreme confinement alone is insufficient to induce ionic memory. Introducing a molecular solvent (such as acetonitrile) or applying compositional asymmetry (salt-concentration gradients) restores pinched hysteresis. These results identify solvent dielectric properties, miscibility, and ion-correlation strength as key control parameters for enabling or suppressing ionic memory in nanochannels, even under strong confinement. Our findings provide both mechanistic insight into ionic memristor behavior and practical methods for controlling hysteresis in nanofluidic devices.

Introduction

Memristors are often described as the fourth fundamental circuit element in addition to resistors, capacitors and inductors [1]. They can “remember” the history of the applied voltage or current. This memory effect is manifested as a pinched hysteresis loop in the current-voltage (I-V) characteristics that pass through the origin [2]. The hysteresis area decreases with increasing frequency and tends toward a single-valued, linear I-V relationship at very high frequencies. Nanofluidic memristors based on liquid electrolytes have recently emerged as ionic alternatives to solid-state memristors for neuromorphic computing [3,4]. Because they use ions instead of electrons, they can operate in physiologically-relevant environments, naturally support multilevel (analog) conductance rather than

only bistable (digital) states [5], and they can display either volatile or non-volatile responses depending on the underlying transport kinetics of the mechanism at the origin of their occurrence. This makes them attractive for interfacing with biological systems, where signalling is ionic, and for implementing synapse-like weights in fluidic or hybrid bioelectronic architectures [6]. The reported mechanisms behind observing memristive effects include: slow adsorption/desorption of ions on channel walls [7]; concentration polarization/depletion that builds asymmetric ion profiles [8]; surface charge inversion or regulation that flips ionic selectivity [9]; transient ion-enrichment and depletion; voltage-gated wetting/dewetting of hydrophobic pores [10]; association/dissociation (Wien-type) ion pairing under strong confinement [11]; biomembrane channel insertion/removal [12,13]; mechanical blistering of 2D stacks [14,15], and in some cases, pseudo-memristance originating from potential-driven Ag electrodeposition/stripping , which reflects electrochemical redox processes at electrodes rather than intrinsic channel memristance [16]. When a voltage is swept, the current does not follow instantaneously because these processes have finite kinetics; the result is a pinched I-V loop whose area and orientation depend on the electrolyte, surface chemistry, and geometry. Most of the experimentally demonstrated systems so far use aqueous electrolytes and simple salts (e.g., KCl, NaCl, $CaCl_2$) in glass or polymer conical pores [17,18], 2D angstrom slits [9], asymmetric SiN_x nanopores [14,19], or functionalized nanochannels [20]. The main memristive mechanisms have been identified so far with nanochannels and aqueous electrolytes.

Ionic memory has been observed in conical nanochannels filled with immiscible RTIL/water interfaces (adsorption/desorption controlled), in arrays of glass nanocapillaries showing ion-concentration polarization (depletion/enrichment controlled) [21], in PDMS nanochannels containing an aqueous/RTIL interface that moves under bias (interfacial-displacement controlled) [22,23], in a Si_3N_4 nanopore-microwell system using an immiscible RTIL/KCl 1M aqueous electrolyte meniscus, where memristive behaviour arises from voltage-induced meniscus expansion and contraction[24], and in PDMS microchannels where redox chemistry of Cu/ionic gel forms and ruptures conductive paths [25,26]. In other words, several mechanisms can produce the same macroscopic signature which is a pinched hysteresis loop and in experimental systems more than one of the mechanisms may be responsible. This diversity is scientifically interesting, but it also generates a problem: it is hard to decouple co-existing mechanisms, and it is still not yet fully established when a confined electrolyte should be expected to show memristive hysteresis and when the I-V curve should remain essentially Ohmic.

The main criterion for ionic memory[4], as described in the literature, is the presence of asymmetry: whether in surface charge, geometry (cone, funnel, entrance effects), or composition (e.g., concentration gradient [27,28], or asymmetric aqueous/IL environments across the nanochannels [21,22,24]). Such asymmetry ensures at least two conduction states exist along the channel and, if the processes that connect those states have different finite kinetics, a hysteresis loop appears. However, even in symmetric systems, phenomena like the Wien-effect can still generate multiple conductance states. In this case, the memory arises from ionic rearrangements within the confined liquid rather than from ion-wall interactions or entrance effects. So, a system in which we can decouple solvent effects and the ion-wall interaction can help in better understanding and thus tuning of nanofluidic memristive phenomena.

RTILs are solvent-free salts made of bulky, often asymmetric ions, with viscosities tens to thousands of times higher than water, conductivities typically 0.1-20 mS/cm (compared to hundreds of mS/cm for aqueous electrolytes), and a strong tendency to form ion pairs and over-screened layers near charged walls [29,30]. Under nanoconfinement, RTILs can crowd, layer, or even enter superionic regimes depending on the pore material [29]. These features directly affect the charging and discharging times that may, under suitable conditions, give rise to memristive hysteresis. However, RTIL-based memristors reported so far often involved an additional condition such as a redox-active electrode, an aqueous/IL interface that can move, or a mixed IL/water composition, and were typically demonstrated in thick nano/microchannels with heights of tens or hundreds of nanometers that normally do not show any memristive effect using aqueous electrolytes [21,22,24]. The development

View Article Online
DOI: 10.1039/D5FD00142K

of aqueous nanofluidic memristors in extremely confined systems (<10 nm) has remained unexplored. The physicochemical characteristics of IL (absence of solvent, high ion density, strong correlations, viscosity, and low conductivity) therefore offers an opportunity to probe the fundamental mechanisms of ionic memory under extreme confinement.

Another gap in the nanofluidic memristors understanding is the role of solvent. Diluting aqueous electrolytes or RTIL with a molecular solvent (acetonitrile, propylene carbonate) other than water has not been reported yet to induce memristive effects. It is known that solvents reorganize the liquid structure, weaken ion pairing, and increase mobility of RTILs up to an intermediate composition, after which the solution becomes solvent-dominated [31]. Because memristive mechanisms depend greatly on breaking the continuum under nanoconfinement where the solvent properties can change, and the interactions of ions with solvent and channel wall change dramatically [32,33], such changes in solvation and transport should translate directly into the presence, absence, or strength of hysteresis. Yet systematic studies that compare the same nanofluidic channel filled with (i) aqueous electrolyte, (ii) pure RTIL, and (iii) RTIL/solvent mixtures under symmetric and asymmetric boundary conditions are still to be done using various confinement systems. Without that comparison, it is difficult to tell which of the reported mechanisms is intrinsic to the liquid and which one is enabled only by an imposed asymmetry in nanochannels.

In this work, we address precisely this point. We take 2D confined nanochannels that we have previously shown to exhibit four distinct memristive loop styles in aqueous electrolytes and we replace the liquid phase with RTIL and RTIL/molecular-solvent mixtures. By controlling surface charge, concentration symmetry, and the nature of the solvent, we map the conditions under which the I-V response keeps its hysteretic characteristics, weakens into a nearly linear curve, or disappears altogether. This approach lets us test the often-stated assumption that “under nanoconfinement we should always expect memory” and to show that this assumption is too strong: confinement favors memory, but solvent-controlled ion correlations and mobility can suppress it. Our goals are therefore threefold: (i) to clarify which of the known ionic memristive mechanisms can operate in a purely IL environment under strong confinement; (ii) to show how introducing or removing solvent tunes the relevant kinetics so that hysteresis can be switched on or off; and (iii) to provide a mechanistic framework that explains why some nanofluidic systems with ILs show rich, multi-level ionic memory, while others of very similar geometry do not.

Experimental

2D Nanochannel geometry

The nanofluidic structure consists of slit-like 2D channels with a uniform cross-section (Figure 1A and Figure S1). Geometrically, each channel can be viewed as a narrow parallelepiped: ions can move freely along the channel length and width, while motion in the vertical direction is confined to a height defined by the spacer, that can vary between ~0.34 nm and several tens of nanometers [34,35]. The device contains on the order of 200 channels arranged in parallel (Figure 1D). The channel height is fixed by the thickness of the 2D spacer layer, graphene (Gr) stripes, and the lateral aperture of the channel is set by the spacing between graphene spacers, giving a width of about ~110 ± 10 nm (Figure 1D). Ion transport can be established from the hole side toward the channel side or in the opposite direction, depending on the applied potential and concentration gradients. Throughout this paper we report heterogeneous mixtures from the hole/device side.

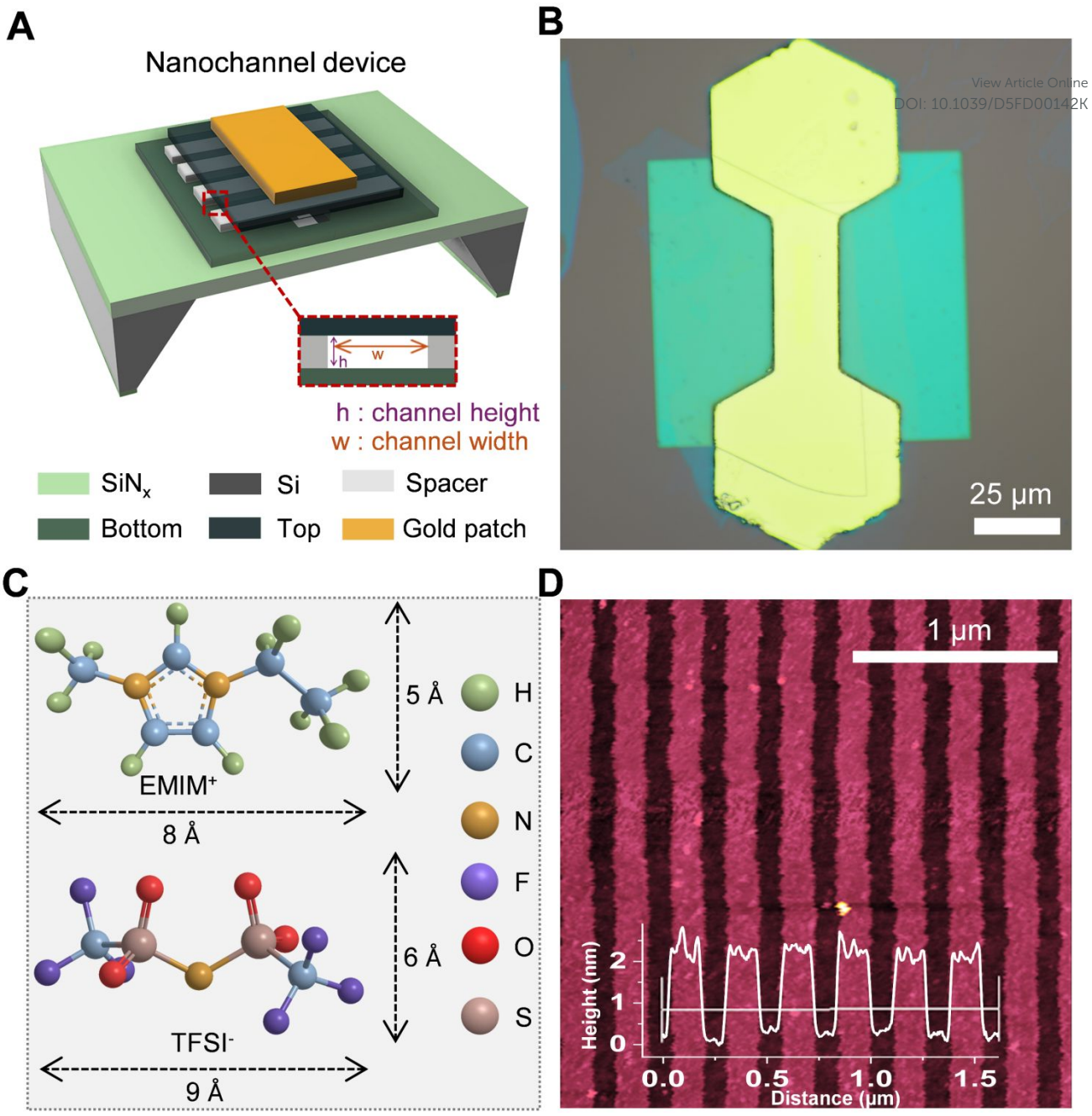

Figure 1: 2D nanochannel device architecture and used room temperature ionic liquid. A) scheme (perspective view) of the 2D nanochannels device composed of top, bottom, and spacer layers over a micro-hole in a silicon nitride (SiN_x) membrane where the electrodes would be from the hole (under silicon) or the channel (above silicon) side.B) Optical microscopy (up-view) of the nanofluidic device covered by gold patch. C) The chemical structure of the RTIL ($EMIM^+$ and $TFSI^-$ ions) showing the dimensions of the cation and anion. D) Atomic force microscopy (AFM) images of the spacers with a width of ~110 nm and a height of 1.94 nm.

Electrochemical / ionic transport measurements

I-V characteristics were recorded using a Biologic S-300 potentiostat controlled by EC-Lab program while using ultra-low current cables. Two electrode system was used as the currents were very small thus yielding a negligeable ohmic drop. The working electrode (WE) was always placed at the hole side denoted by V_{WE}, while the reference and counter electrodes (RE/CE) were placed at the device side denoted by $V_{CE/RE}$. Ag/AgCl electrodes were used while results were compared using aqueous electrolyte using Pt and Ag/AgCl pseudo electrodes and no variation of the memristive effect was observed as the effect is mainly due to the passage of ions inside the nanochannels rather than redox activity at the electrode's surface (Figure S5). The two electrodes were placed on both sides of the fluidic chamber designed to host only 100µL of the RTIL over both sides of the nanocapillary

device. Cyclic voltammetry was performed using a triangular voltage waveform over the potential ranges indicated in each figure, at scan rates corresponding to frequencies between 0.625 mHz and 1.25 Hz, calculated based on the time required to complete one full cycle starting from 0 V versus an Ag/AgCl pseudo-reference electrode. Performing three cycles did not result in significant variation in the absolute current and very small variation in the hysteresis area (Figure S7). One of the graphs among the repeated cycles is presented.

View Article Online
DOI: 10.1039/D5FD00142K

Before ionic memory measurements with aqueous electrolytes [36], the cell was rinsed thoroughly with deionized water then with the designated solution, while for IL washing was done with Acetonitrile (99.9%) several times then with the RTIL solution. All measurements were carried out with the device and electrodes enclosed in a Faraday cage to minimize electrical noise and improve signal stability.

Synthesis of RTIL:

The ionic liquid, 1-ethyl-3-methylimidazolium bis(trifluoromethylsulfonyl)imide ([EMIM][TFSI]), was synthesized as described elsewhere [37,38] via a metathesis reaction between 1-ethyl-3-methylimidazolium chloride ([EMIM][Cl]) (75 g, 0.51 moles) and lithium bis(trifluoromethylsulfonyl)imide (LiTFSI) (154 g, 0.54 moles) (Figure 1C). The starting materials were obtained from Sigma-Aldrich and used without further purification.

In a typical procedure, approximately equimolar quantities of [EMIM][Cl] and LiTFSI were dissolved in deionized water (100 mL) and magnetically stirred at 40°C for 12 h to allow complete ion exchange. The reaction mixture was then separated into two phases over a funnel: the upper aqueous phase containing LiCl and the lower viscous phase containing the target ionic liquid [EMIM][TFSI]. The ionic liquid phase was repeatedly washed with deionized water having a volume at least twice as the volume of RTIL and the whole washing process is repeated at least 10 times to ensure that LiCl impurities were completely removed. The absence of chloride ions was detected in the washings, as confirmed by silver nitrate ($AgNO_3$) precipitation tests. The washed [EMIM][TFSI] was then dried under vacuum (<$6x10^{-2}$ bar) at 70 °C for 3 days to remove residual water.

Results and discussions

Four distinct memristive loop styles could be generated under nanoconfinement where their occurrence depends on channel height, electrolyte valency and concentration, surface charge and selectivity of the channel walls [9]. Here, we first tested aqueous electrolytes, KCl, LiTFSI (chosen because $TFSI^-$ anion is well studied and used in many RTILs), and H_2SO_4, using 2D nanofluidic channels (h= 1.3 nm). For 1M KCl and LiTFSI solutions, we now observe a Wien-type behavior, which we attribute to the field-induced dissociation of non-conductive Bjerrum pairs into conductive species (polyelectrolyte and free ions), leading to multilevel conductance states (Figure 2 A & B). The surface charge and the ion selectivity of the nanochannel affected the rectification factor (ratio of positive to negative current obtained at similar positive and negative voltages). In contrast, for H_2SO_4, which is a strongly acidic electrolyte, we mainly observed a crossing-1 type mechanism: two conductance states appeared, corresponding to ion enrichment and depletion in an asymmetric channel (geometric and/or surface-charge asymmetry) (Figure 2 C). In this case, the hysteresis is better explained by different adsorption/desorption kinetics of the co-ion (or the counterion in crossing-2 situations). The magnitude and polarity of rectification depend on the device state, which is governed by the geometric asymmetry and by the effective surface charge of the nanochannels, both of which control ionic selectivity[39,40]. Ions of different nature, with distinct physico-chemical properties, exhibit different selectivity and field-driven transport behavior under confinement[33]. In addition, ion concentration, ion type and valency can modify the effective surface charge through charge regulation and, in some systems, surface charge inversion, thereby altering the rectification. Similar rectification inversion and selectivity switching with salt concentration and ion identity have been reported previously in angstrom-scale channels[9].

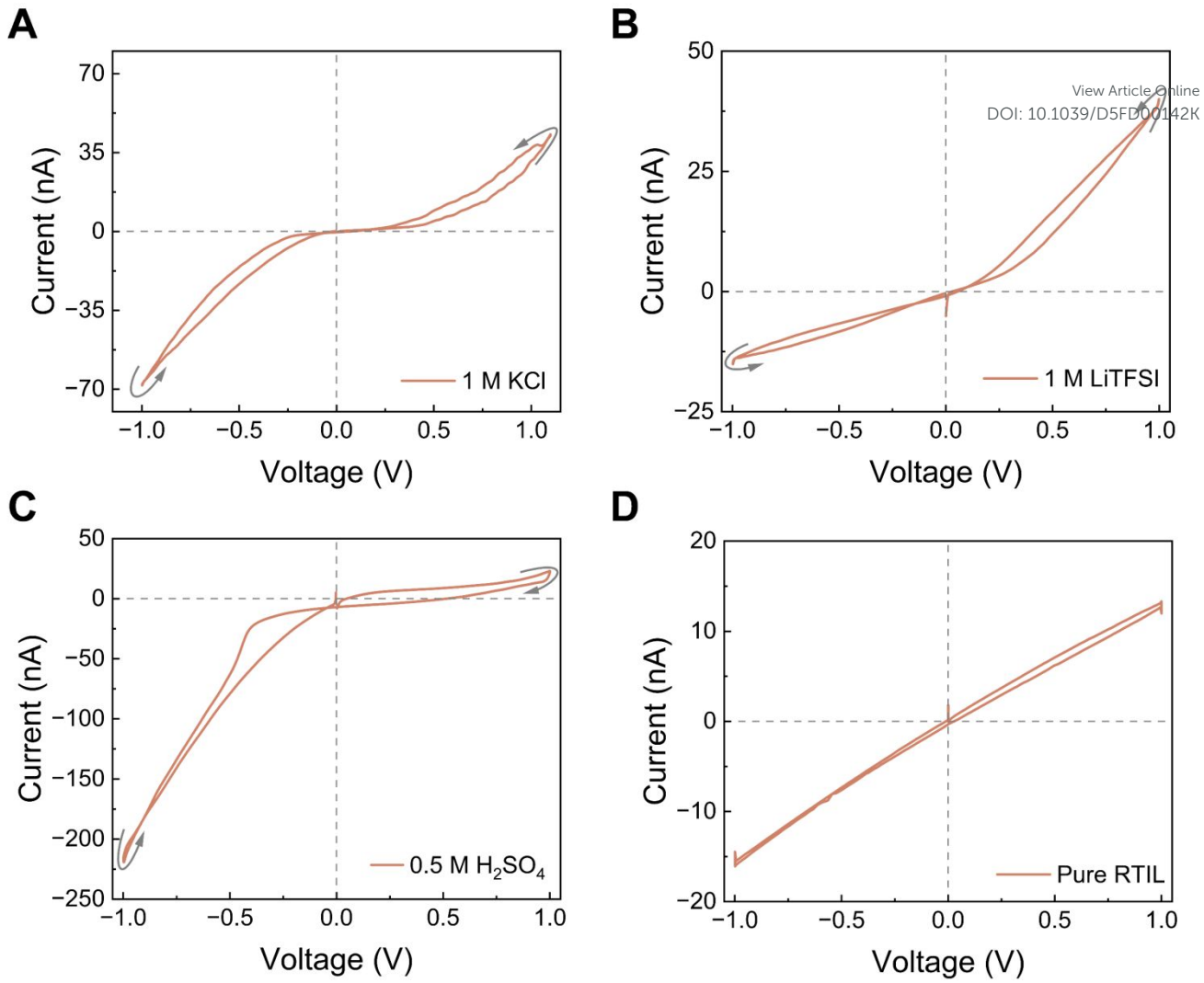

Figure 2: Ionic memory hysteresis loops for several aqueous electrolytes and for RTIL. Different electrolytes were used A) aqueous 1M KCl , B) aqueous 1M LiTFSI, C) aqueous 0.5M H_2SO_4, and D) pure EMIM-TFSI RTIL. The memory styles were in A) Crossing 1 and B-C) Wien-type, whereas in D) Pure ionic liquid shows capacitive loops, without pinching at the origin. All electrolytes were tested by cyclic voltammetry using a triangular voltage waveform with a scan rate of 20 mV/s (equivalent to a frequency of 5 mHz). Measurements were performed in an hBN/graphene/hBN (top/spacer/bottom) device with a channel height h= 0.7 nm, corresponding to the graphene spacer thickness.

When we replaced the aqueous electrolytes by pure EMIM-TFSI RTIL, the I-V curves showed only a capacitive loop that did not pinch (Figure 2 D). Changing the scan rate modified the loop area, as expected for a capacitive system, but at no frequency did we observe a pinched hysteresis characteristic of memristors. This suggests that, unlike aqueous electrolytes, the confined RTIL did not generate distinct subpopulations with different conductivities, i.e. there was no effective “switch” between low- and high-conductance states and only one conductance state existed. This could be due either to the absence of Bjerrum-pair formation/dissociation in this geometry, or more plausibly to the fact that, although ion pairing is favored in RTILs (low dielectric constant, no solvent), these pairs do not undergo the same field-assisted dissociation pathway as in water. RTILs under nanoconfinement are known to undergo several structural regimes, from superionic states in pores comparable to the ion size (with enhanced mobility), to glassy, layered states in ultranarrow or strongly adsorbing pores, where mobility is strongly reduced [29]. In such conditions, ion-ion and ion-wall interactions are highly correlated and governed by the nature of the confining walls [41]. Our results therefore point to an important conclusion: the presence of a solvent phase, with a dielectric constant higher than that of the RTIL and different inside vs outside the nanochannel, seems to be essential for observing a Wien-type memristive behavior for a tested electrolyte. In neat RTIL, the very high ionic concentration, the specific double-layer structure (overscreening/crowding), and the

comparatively low conductivity can all suppress the parameters that produced memristance of electrolytes in water: (i) polyelectrolyte formation, (ii) entrance ion concentration polarization, and (iii) rectification arising from asymmetric access resistance or channel geometry/charge. Without those, none of the four memristive effects previously identified in aqueous electrolytes could be triggered, and no memristance was observed even under extreme confinement.

To isolate the role of the solvent in enabling memristive behavior, we next used LiTFSI as a model electrolyte in different solvents. LiTFSI has the same anion ($TFSI^-$) as the RTIL (EMIM-TFSI) tested above, but unlike the RTIL it is readily soluble in several solvents including water. When LiTFSI was dissolved in water at 1 M and confined in our 2D nanochannels, we obtained a Wien-type memristor, as expected from our previous aqueous results (Figure 3 A). This indicates that, under confinement, Li^+ and $TFSI^-$ can form Bjerrum pairs that are partially dissociated by the electric field, giving rise to more conductive polyelectrolyte-like species and to multilevel conductance. Here the high bulk dielectric constant of water ($\varepsilon \sim 80$), which is known to decrease strongly under confinement [42,43], still remains high enough to allow field-assisted dissociation. We then replaced water by acetone, a solvent that also dissolves LiTFSI but has a ~4x lower bulk dielectric constant ($\varepsilon \approx 21$) , which can decrease further in a few-nanometer slit [44]. In this case we still observed a pinched loop, but the dominant memristive behavior was of the saturation type and the overall conductivity was about four times higher (Figure 3 B). This change in loop style can be rationalized by a stronger contribution of ion-concentration polarization at the channel entrance (depletion/enrichment) and a weaker Wien-type contribution: with a lower-permittivity solvent the contrast between “paired” and “field-dissociated” states is smaller, so the ICP mechanism becomes comparatively more visible. It is also worth noting that the conductance of LiTFSI in acetone increases by more than 4 times compared to the aqueous phase. This behaviour is not unexpected as acetone ($\eta = 0.306\ at\ 25°C$) has a viscosity ~3 times lower than that of water ($\eta = 0.89cP\ at\ 25°C$) [45], which enhances ion mobility and therefore conductivity both in bulk and in nanochannels. The faster ion mobility likely facilitates the formation of ICP associated regime. Finally, we dissolved LiTFSI (1 M) directly in the ionic liquid ($\varepsilon \approx 12$ [46,47]) and repeated the measurements. In this medium, no memristive effect was detected (neither Wien-type nor saturation-type) exactly as in the case of the neat RTIL (Figure 3 C). Lowering the LiTFSI concentration in the RTIL to 0.1 M did not restore the pinched hysteresis (Figure 4 A). This shows that the lack of memristance in the RTIL system is not due to the specific identities of Li^+ or $TFSI^-$, but to the physicochemical properties of the RTIL itself (high ion density, low permittivity, strong ion-ion correlations) which suppress the mechanisms that, in water or acetone, generate multiple conductance states. We also note that adding LiTFSI to the RTIL decreased the overall conductance, consistent with ion crowding and the formation of additional non-conductive ion pairs (Figure 2 D, 3 C, & 4 A). Although this is a drawback for device conductance, it actually provides a clean platform to disentangle which parameter (solvent permittivity, entrance polarization, and field-induced dissociation) are strictly required to observe nanofluidic memristance under extreme 2D confinement.

We have observed non-zero crossing or potential shifts of the I-V curves at certain conditions mainly using non-aqueous electrolytes. This shift has been reported previously in nanofluidic systems and can arise from delayed ionic relaxation, including double-layer charging and concentration polarization, when the ion distribution cannot fully equilibrate during the voltage sweep[17,48-51]. In non-aqueous electrolytes, strong ion-ion correlations and slow redistribution further enhance this effect, leading to a more pronounced offset. In addition, the use of quasi-reference electrodes in such media may introduce potential offsets due to electrode polarization, which can contribute to non-zero crossing in cases where no clear memristive hysteresis is observed[52].

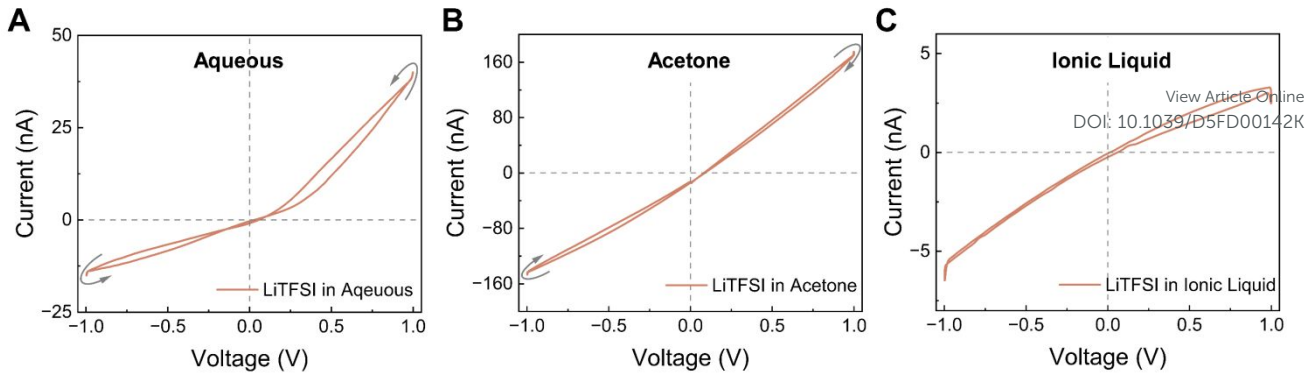

Figure 3: Effect of the solvent medium on LiTFSI electrolyte IV curve. A 1 M concentration of LiTFSI was dissolved in A) water, B) acetone, and C) the room-temperature ionic liquid EMIM-TFSI. Memristive hysteresis loops in Wien and saturation style were observed in A) and B), respectively, whereas purely capacitive, non-pinched loop was observed in C). All electrolytes were tested by cyclic voltammetry using a triangular voltage waveform with a scan rate of 20 mV/s (equivalent to a frequency of 5 mHz). Measurements were performed in an hBN/graphene/hBN (top/spacer/bottom) device with a channel height h= 0.7 nm, corresponding to the graphene spacer thickness.

When we imposed an asymmetric salt gradient of LiTFSI while keeping EMIM-TFSI (RTIL) as the solvent, the nanochannel exhibited a crossing-2 type memristor (Figure 4 B & C). Whether one reservoir contained no added salt and the other did (Figure 4 B), or both reservoirs contained electrolyte but at different concentrations (Figure 4 C), the asymmetry was enough to generate two distinct conductance states. The most plausible origin is that the two sides of the channel experienced different ion populations and interactions and therefore different enrichment/depletion of conducting entities inside the nanochannel. This kinetic asymmetry, similar to the concentration-gradient-driven memristive switching observed in conical nanofluidic diodes [28], produced a pinched I-V loop whose area depended on the scan frequency, a defining feature of memristive behavior. The small dimensions of the nanochannels, which limit the permeability of diffusing ions, ensure that the bulk concentrations of ions in both reservoirs remain effectively unchanged during the measurement [32,35]. Similar to aqueous systems where a concentration gradient is imposed across the nanochannel [9], here a gradient exists for $TFSI^-$ and Li^+ ions across the RTIL-filled channel. Because the ion concentrations differ on the two sides, diffusion establishes a steady concentration profile inside the nanochannel [53]. This diffusive flux is further modulated by the polarity of the applied voltage, which drives $TFSI^-$ or Li^+ selectively depending on the bias polarity, consistent with voltage-dependent accumulation/depletion mechanisms described in concentration-gradient nanochannels [53].

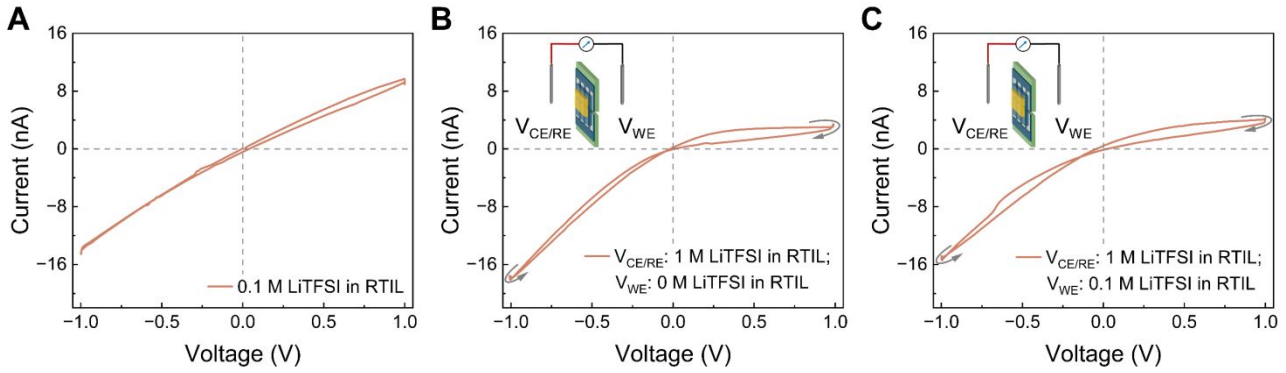

Figure 4: Effect of symmetric/asymmetric conditions of electrolyte in producing memory. Different electrolytes were tested under (A) symmetric and (B, C) asymmetric conditions. A) LiTFSI was dissolved in the RTIL (EMIM-TFSI) at concentrations of 0.1 M. Asymmetric conditions were made by adding LiTFSI at different concentrations across the device B) 0 M LiTFSI in RTIL (hole side) / 1 M LiTFSI in RTIL (device side), and C) 0.1 M LiTFSI in RTIL (hole side) / 1 M LiTFSI in RTIL (device side). Under these asymmetric conditions (B and

C), the observed memristive behavior corresponded to a crossing-1 type loop, whereas only capacitive I-V curves without pinching were observed under symmetric conditions (Panel A, and figures 2 D, 3 C). All electrolytes were tested by cyclic voltammetry using a triangular voltage waveform with a scan rate of 20 mV/s (equivalent to a frequency of 5 mHz for ±1V voltage range). Measurements were performed in an hBN/graphene/hBN (top/spacer/bottom) device with a channel height h= 0.7 nm, corresponding to the graphene spacer thickness.

To probe this mechanism further, we diluted the ionic liquid in various solvents. As discussed above, neat RTIL is an ion-only medium with low permittivity; adding a molecular solvent of higher permittivity will increase the effective dielectric constant and can weaken ion-ion correlations [54]. We therefore asked whether, upon dilution, EMIM-TFSI would start to behave like a “normal” electrolyte and recover the memristive effects we routinely observe in water. EMIM-TFSI is not miscible with water, so we used acetonitrile which has a bulk permittivity of 38 that decreases to 7 in nanochannels of h= 1.4 nm [44]. At a low RTIL concentration (10 mM ET in acetonitrile) the response was purely capacitive: the loop did not pinch at the origin (Figure 5 A). However, increasing the concentration to 0.1 M produced a clear crossing-2 memristive loop (Figure 5 B). This indicates that, at this concentration, two conductance states exist and the cation ($EMIM^+$) can reversibly adsorb/desorb on the channel walls, exactly as we saw for dilute aqueous salts [9]. Increasing the IL concentration further to 0.5 M generated a double-crossing loop, which we interpret as the coexistence of two mechanisms : a crossing-2 process (adsorption/desorption of the co-ion on an asymmetric channel) and a Wien-type contribution (field-assisted change in the population of conducting species) (Figure 5 C) [7]. Such mixed loops were also observed previously in aqueous electrolytes at intermediate concentrations. At 1 M EMIM-TFSI, the loop evolved into a crossing-1 type, consistent with a partial surface-charge inversion and adsorption/desorption now dominated by the anion ($TFSI^-$) (Figure 5 D). When the IL concentration was increased beyond 2.9 M (approaching the neat RTIL), all pinched hysteresis disappeared and only a non-pinched capacitive loop remained (Figure 5 E). In other words, as the electrolyte became more RTIL-like again (high ion density, low dielectric constant, strong correlations), the nanofluidic memristive effects were suppressed. Finally, performing the same dilution experiments in solvents other than acetonitrile, such as dimethyl carbonate and diethyl carbonate, led only to capacitive behavior, with no pinched loops (Figure S6). This comparison confirms that the solvent’s dielectric and interfacial properties are crucial: only when the ionic liquid is diluted in a medium that can partially release ion-ion correlations do the adsorption-controlled nanofluidic memristor mechanisms re-emerge.

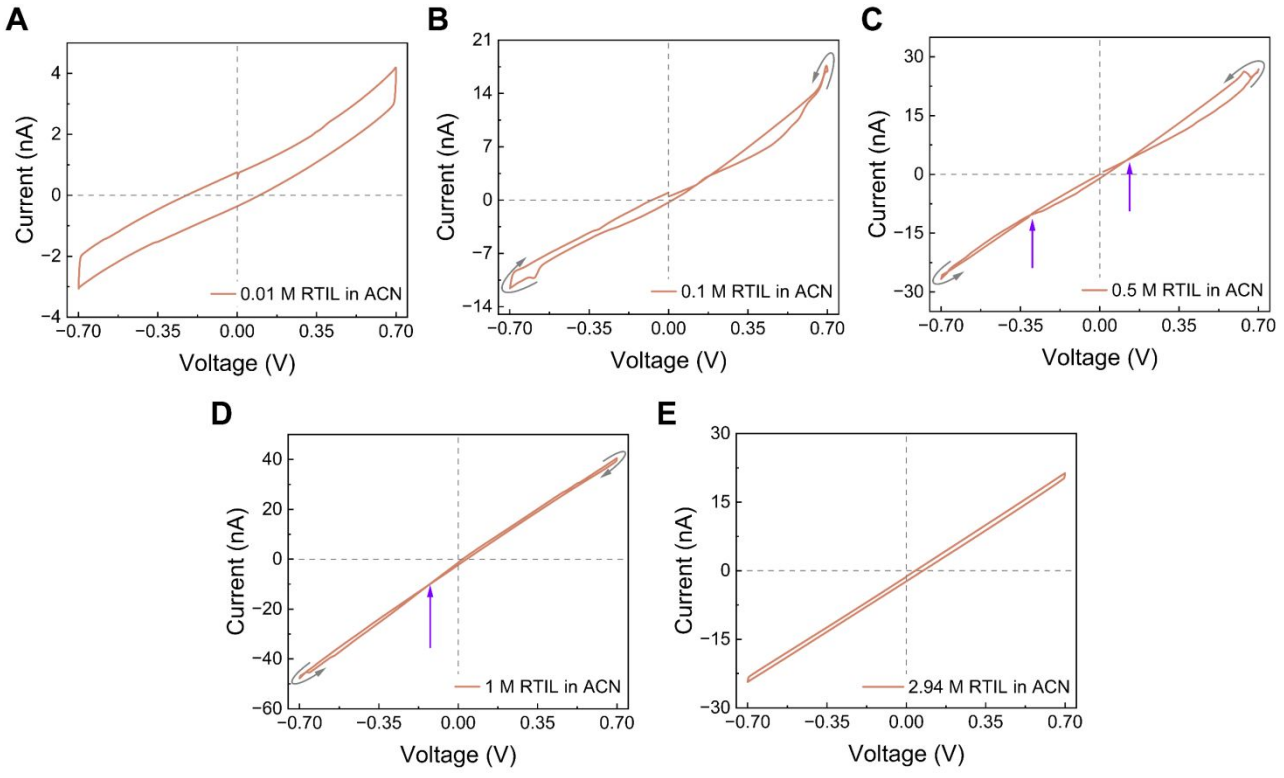

Figure 5: Effect of dilution of ionic liquid in Acetonitrile solvent. Various concentration of Ionic liquid diluted in acetonitrile were tested A) 0.01M, B) 0.1M, C) 0.5M, D) 1M, and E) 2.94M. A) and E) showed only capacitive curve without pinched loop. B) showed crossing 2 memristor, C) showed double crossing Wien-type and crossing 2, D) crossing 1. All electrolytes were tested by cyclic voltammetry using a triangular voltage waveform with a scan rate of 20 mV/s (equivalent to a frequency of 7.1 mHz). Measurements were performed in hBN/graphene/graphene (top/spacer/bottom) device with a channel height h= 1.4 nm, corresponding to the graphene spacer thickness.

As the asymmetry is described as a key parameter in the observed memristive effects, as well as our observation of the appearance of memory in system, we decided to further investigate if asymmetry always led to memory. To test this, we introduced a solvent asymmetry by filling one reservoir with neat EMIM-TFSI and the other with acetonitrile. Under this condition, the device showed a crossing-1 type loop (Figure 6 D). This asymmetric condition was established after characterizing the nanochannels under symmetric RTIL conditions and then replacing the RTIL on the hole side with ACN. The amplitude of the measured current did not change during the measurements while testing the frequency effect on IV for ~15 minutes, indicating that the RTIL/ACN interface did not undergo big variation that affect our conclusions under the tested conditions. Mass transport in this configuration is governed by (i) the concentration gradient driving both ions from the device side toward the hole side, and (ii) the electric field, which pushes $TFSI^-$ toward the ACN side under positive bias and $EMIM^+$ under negative bias. Since RTIL and ACN are fully miscible, a gradual spatial variation of ion concentrations is expected. The extent of this gradient depends on the degree of nanochannel filling by the RTIL, dictated by wetting and interfacial interactions, and on the competition between ACN, the RTIL phase, and individual ions under both concentration and electric-field gradients. The bulk ACN can pass electric current under these conditions despite showing no current when both sides were filled with ACN, suggesting that some ions have already diffused from the EMIM-TFSI compartment through the nanochannels. The positive current was smaller in magnitude than the negative current, which is consistent with the lower mobility of the IL cation ($EMIM^+$) compared with the $TFSI^-$. When we replaced acetonitrile by pure water (without KCl), the I-V curve became purely capacitive, i.e. no memory was observed (Figure 6 C). This indicates that miscibility between the RTIL and the other liquid, and the resulting differential diffusion of ions across the interface, are necessary for the memristive response. It should be noted that each solvent alone did not show any memristive effect (Figures 6 A-C)

We then tested a different asymmetry: an aqueous KCl on one side and neat RTIL on the other. In this configuration, the I-V curves showed a double-crossing loop at higher voltages, which implies the coexistence of two memory mechanisms (Figure 6 E & F). At lower voltages only crossing 1 memory effect appeared (Figure 6 G & H). Since neither pure water nor neat RTIL alone produce hysteresis in this device, the new loops must arise from the coupled migration of K^+ / Cl^- and $EMIM^+$ / $TFSI^-$ ions across the RTIL/aqueous interface and from the reorganization of that interface under potential bias. This behaviour is broadly consistent with other nanoscale studies of heterogeneous liquid pairs confined in nanopores or nanochannels (tens of nanometers high), where electrokinetic interface displacement or directional ion transport between immiscible phases can produce history-dependent conductance [21,22,24]. However, an important difference is that in our 2D nanochannels, one or more of four loop styles always exist for aqueous electrolytes, whereas in many of those nanoconfinement studies no memory is seen with aqueous solutions of electrolytes. This implies that the balance of forces in our 2D confinement, where steric, ionophilic, and electrostatic interactions are magnified, is different.

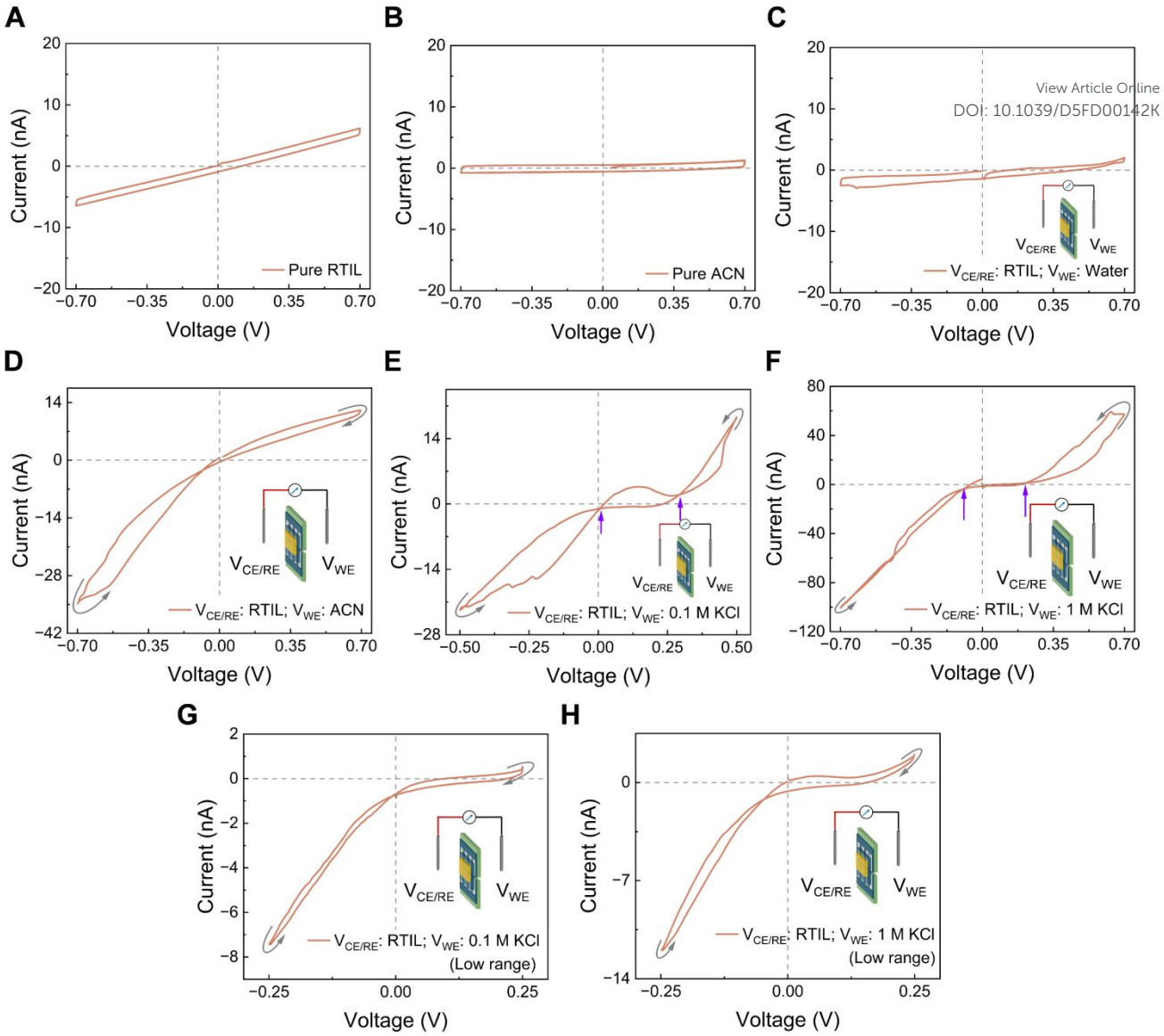

Figure 6: Effect of asymmetric solutions on the generation of memristive behavior A) pure EMIM-TFSI (RTIL) and B) pure acetonitrile were tested under symmetric conditions on both sides of the 2D nanochannels. Asymmetric conditions were made by placing RTIL on the device side while the hole side contained: C) pure water or D) pure acetonitrile. The hole-side solution was then replaced with E,G) 0.1 M KCl or F,H) 1 M KCl, while keeping RTIL on the device side. Measurements in E-F were performed at 0.7 V, and those in G-H at a lower voltage range of 0.25 V. No memristive behavior was observed in A-C, whereas crossing-1 loops appeared in D, G, and H. Double-crossing loops (placed at up-arrows) showing Wien-type and crossing-1 styles were observed in E and F. All electrolytes were tested by cyclic voltammetry using a triangular voltage waveform with a scan rate of 40 mV/s. Measurements were performed in an hBN/graphene/graphene (top/spacer/bottom) device with a channel height h= 1.4 nm, corresponding to the graphene spacer thickness.

Overall, the asymmetric aqueous-RTIL configuration produced a mixed memristive behavior that can be interpreted as the superposition of a Wien-type mechanism and a crossing-2 mechanism. Under a positive bias applied from the hole side to the device side, $TFSI^-$ anions in the RTIL (device side) are driven toward the aqueous phase (hole side), while K^+ ions from the aqueous reservoir (hole side) are pushed into the RTIL-rich region (device side). Under a negative bias applied from the device side to the hole side, $EMIM^+$ cations in the RTIL (device side) migrate toward the aqueous phase (hole side). In contrast, only a limited flux of Cl^- ions (or K^+ under opposite polarity) can enter the RTIL-rich region because this transfer is thermodynamically unfavorable: Cl^- (or K^+) must partially dehydrate and has intrinsically poor solubility in the RTIL. In both bias directions, the relative magnitudes of these ion fluxes are dictated by their solvation energies and their partitioning equilibria

between the aqueous and RTIL phases. Hydrated ions (K^+, Cl^-) preferentially remain in the aqueous phase, whereas $EMIM^+$ and $TFSI^-$ exhibit strong affinity for the RTIL, leading to strongly asymmetric transfer kinetics under opposite biases. Additional contributions arise from viscosity variation affecting ion mobility in both phases and resulting in diffusion currents, liquid-liquid junction potential, and interface displacement under potential bias[55]. Under zero applied bias, the equilibrium position of the aqueous/RTIL interface inside the nanochannel is primarily determined by the wettability and interfacial energies of the two liquids with the channel walls. Ion-wall interactions (ionophilicity or ionophobicity) further modulate how each ion anchors to the surface, influencing whether water or RTIL preferentially occupies the confined region and how sharply the interface is defined[55].

Regarding ion affinity, $TFSI^-$ has been shown to interact more strongly than chloride with graphite and it intercalates readily [38]. However, the nature of the channel walls can modify this affinity [41]. In our experiments, the channels were initially filled with RTIL on both sides; ACN was then introduced on the hole side, followed by water and finally $KCl_{(aq)}$. Nevertheless, the precise position of the RTIL/aqueous interface, and how it may shift under applied potential, requires further investigation including those with imaging techniques. Several hypotheses may explain the origin of the observed memory: displacement of the RTIL/aqueous interface inside the channel or at its entrances (from the hole or device side), ion concentration polarization, or bias-dependent variation in ion adsorption on the 2D material surfaces. In all cases, these effects translate into different resistances at the two channel entrances, and the bias-dependent composition of the nanoconfined solution collectively gives rise to the two observed conductance states. When same conditions were applied to a delaminated device showing no confinement, a saturation-like pinched loop was observed (Fig S4). This is similar to pinched loops observed in literature for thick channels [21-23]. The observation of mixed loops (Wien-type & Crossing) in our channels, suggests that nanochannels play a role in this memory and not their entry as is the case of delaminated channels.

Table 1: Conditions Leading to Memristive vs. Non-Memristive Behavior

No memristor	Memristor
Pure ionic liquid, or ionic liquid diluted in most solvents (ex. diethyl carbonate, dimethyl carbonate, acetone...), under confinement	Ionic liquid diluted in acetonitrile (0.1 to 1M) in confinement
No confinement of aqueous electrolyte solution (thick channels)	Aqueous electrolyte solution under confinement
Asymmetric condition of IL/water	Asymmetric conditions of: • IL/aqueous electrolyte • IL/solvent • IL/IL diluted in solvent • IL/electrolyte dissolved in IL
Symmetric electrolyte in Ionic liquid	

Conclusion

This work shows that nanoconfinement by itself does not guarantee ionic memory: aqueous electrolytes in our 2D channels can show all four known I-V loop styles, but the same geometry filled with neat EMIM-TFSI shows purely capacitive I-Vs. By replacing water with lower-permittivity solvents, or by diluting the ionic liquid, we could gradually “turn back on” adsorption- and Wien-type mechanisms, demonstrating that solvent dielectric properties and ion-ion correlations are control knobs behind the appearance, the type, and the strength of the hysteresis (table 1). Asymmetry helps only when it produces two conductance states with different relaxation times; otherwise, it remains capacitive. These results provide a simple design rule for nanofluidic neuromorphic elements: pick a solvent (or mixture) that allows field-assisted ionic rearrangement, then add

geometric or compositional asymmetry to stabilize the memory state. These results open a pathway to further studies to test how different materials especially with different conductivities interact with RTIL. Simulation studies could complement the observed phenomena by including the effect of solvents on memory prediction and testing of other RTIL of various miscibilities and physico-chemical characteristics (dielectric response, conductivity, viscosity, layering, solvation, water affinity, etc.) and composition (cation/anion combinations) could give further mechanistic insights into memory generation.

View Article Online
DOI: 10.1039/D5FD00142K

References

1 Chua, L. Memristor-The missing circuit element. *IEEE Trans. Circuit Theory* **18**, 507-519, doi:10.1109/TCT.1971.1083337 (1971).

2 Chua, L. If it's pinched it's a memristor. *Semiconductor Science and Technology* **29**, 104001 (2014).

3 Xu, G. *et al.* Nanofluidic ionic memristors. *ACS Nano* **18**, 19423-19442 (2024).

4 Zhou, J., Li, H. & Hou, Y. Chemical Principles in Regulating Nanofluidic Memristors. *Chemistry* **7**, 133 (2025).

5 Li, Y. *et al.* Analog and Digital Bipolar Resistive Switching in Solution-Combustion-Processed NiO Memristor. *ACS Applied Materials & Interfaces* **10**, 24598-24606, doi:10.1021/acsami.8b05749 (2018).

6 Noy, A. & Darling, S. B. Nanofluidic computing makes a splash. *Science* **379**, 143-144 (2023).

7 Robin, P. *et al.* Long-term memory and synapse-like dynamics in two-dimensional nanofluidic channels. *Science* **379**, 161-167 (2023).

8 Bu, Y., Ahmed, Z. & Yobas, L. A nanofluidic memristor based on ion concentration polarization. *Analyst* **144**, 7168-7172 (2019).

9 Ismail, A. *et al.* Programmable memristors with two-dimensional nanofluidic channels. *Nature Communications* **16**, 7008 (2025).

10 Siwy, Z. S., Powell, M. R., Kalman, E., Astumian, R. D. & Eisenberg, R. S. Negative Incremental Resistance Induced by Calcium in Asymmetric Nanopores. *Nano Letters* **6**, 473-477, doi:10.1021/nl0524290 (2006).

11 Robin, P., Kavokine, N. & Bocquet, L. Modeling of emergent memory and voltage spiking in ionic transport through angstrom-scale slits. *Science* **373**, 687-691 (2021).

12 Najem, J. S. *et al.* Memristive ion channel-doped biomembranes as synaptic mimics. *ACS Nano* **12**, 4702-4711 (2018).

13 Koner, S., Najem, J. S., Hasan, M. S. & Sarles, S. A. Memristive plasticity in artificial electrical synapses via geometrically reconfigurable, gramicidin-doped biomembranes. *Nanoscale* **11**, 18640-18652 (2019).

14 Emmerich, T. *et al.* Nanofluidic logic with mechano–ionic memristive switches. *Nature Electronics* **7**, 271-278 (2024).

15 Ismail, A. & Radha, B. Mechano-ionic memristors for nanofluidic logic. *Nature Electronics* **7**, 258–259, doi:10.1038/s41928-024-01150-y (2024).

16 Chen, C. *et al.* Silver Electrodeposition from Ag/AgCl Electrodes: Implications for Nanoscience. *Nano Letters* **25**, 9427-9432, doi:10.1021/acs.nanolett.5c01929 (2025).

17 Wang, D. *et al.* Transmembrane potential across single conical nanopores and resulting memristive and memcapacitive ion transport. *Journal of the American Chemical Society* **134**, 3651-3654 (2012).

18 Wang, D. *et al.* Hysteresis Charges in the Dynamic Enrichment and Depletion of Ions in Single Conical Nanopores. *ChemElectroChem* **5**, 3089-3095, doi:https://doi.org/10.1002/celc.201800571 (2018).

19 Tsutsui, M. *et al.* Transmembrane voltage-gated nanopores controlled by electrically tunable in-pore chemistry. *Nature Communications* **16**, 1089, doi:10.1038/s41467-025-56052-0 (2025).

20 Xiong, T. *et al.* Neuromorphic functions with a polyelectrolyte-confined fluidic memristor. *Science* **379**, 156-161 (2023).

21 Sheng, Q., Xie, Y., Li, J., Wang, X. & Xue, J. Transporting an ionic-liquid/water mixture in a conical nanochannel: a nanofluidic memristor. *Chemical Communications* **53**, 6125-6127 (2017).

22 Li, P. *et al.* Artificial funnel nanochannel device emulates synaptic behavior. *Nano Letters* **24**, 6192-6200 (2024).

23 Zhang, P. *et al.* Nanochannel-based transport in an interfacial memristor can emulate the analog weight modulation of synapses. *Nano Letters* **19**, 4279-4286 (2019).

24 Liu, W. *et al.* A droplet memristor with ionic liquid-electrolyte meniscus. *Chemical Engineering Journal* **504**, 158948 (2025).

25 Khan, M. U., Hassan, G. & Bae, J. Soft ionic liquid based resistive memory characteristics in a two terminal discrete polydimethylsiloxane cylindrical microchannel. *Journal of Materials Chemistry C* **8**, 13368-13374 (2020).

26 Chougale, M. Y. *et al.* Memristive switching in ionic liquid–based two-terminal discrete devices. *Ionics* **25**, 5575-5583 (2019).

27 Liu, K. *et al.* Resistance-Restorable Nanofluidic Memristor and Neuromorphic Chip. *Nano Letters* **25**, 6530-6538 (2025).

28 Ramirez, P. *et al.* Memristive switching of nanofluidic diodes by ionic concentration gradients. *Colloids and Surfaces A: Physicochemical and Engineering Aspects* **698**, 134525 (2024).

29 Kondrat, S., Feng, G., Bresme, F., Urbakh, M. & Kornyshev, A. A. Theory and simulations of ionic liquids in nanoconfinement. *Chemical Reviews* **123**, 6668-6715 (2023).

30 Bresme, F., Kornyshev, A. A., Perkin, S. & Urbakh, M. Electrotunable friction with ionic liquid lubricants. *Nature Materials* **21**, 848-858 (2022).

31 Cruz, C. & Ciach, A. Phase transitions and electrochemical properties of ionic liquids and ionic liquid—Solvent mixtures. *Molecules* **26**, 3668 (2021).

32 You, Y. *et al.* Angstrofluidics: walking to the limit. *Annual Review of Materials Research* **52**, 189-218 (2022).

33 Goutham, S. *et al.* Beyond steric selectivity of ions using ångström-scale capillaries. *Nature Nanotechnology* **18**, 596-601 (2023).

34 Radha, B. *et al.* Molecular transport through capillaries made with atomic-scale precision. *Nature* **538**, 222-225 (2016).

35 Bhardwaj, A. *et al.* Fabrication of angstrom-scale two-dimensional channels for mass transport. *Nature Protocols* **19**, 240-280 (2024).

36 Goutham, S. *et al.* Electric Field Mediated Unclogging of Angstrom-Scale Channels. *Small Methods*, 2400961 (2024).

37 Yang, J. *et al.* Measuring the Capacitance of Carbon in Ionic Liquids: From Graphite to Graphene. *The Journal of Physical Chemistry C* **128**, 3674-3684 (2024).

38 Papaderakis, A. A. *et al.* Anion intercalation into graphite drives surface wetting. *Journal of the American Chemical Society* **145**, 8007-8020 (2023).

39 Nekoubin, N., Hardt, S. & Sadeghi, A. Improved ionic current rectification utilizing cylindrical nanochannels coated with polyelectrolyte layers of non-uniform thickness. *Soft Matter* **20**, 3641-3652 (2024).

40 Qiao, N., Zhang, Z., Liu, Z., Lu, W. & Li, C. Ion current rectification in asymmetric nanochannels: Effects of nanochannel shape and surface charge. *International Journal of Heat and Mass Transfer* **208**, 124038 (2023).

41 Nesterova, I., Kondratyuk, N., Budkov, Y., Gerke, K. & Khlyupin, A. The role of surface material properties on the behavior of ionic liquids in nanoconfinement: A critical review and perspective. *arXiv preprint arXiv:2410.08721* (2024).

42 Wang, R. *et al.* In-plane dielectric constant and conductivity of confined water. *Nature* **646**, 606-610, doi:10.1038/s41586-025-09558-y (2025).

43 Fumagalli, L. *et al.* Anomalously low dielectric constant of confined water. *Science* **360**, 1339-1342, doi:doi:10.1126/science.aat4191 (2018).

44 Ronceray, N. *et al.* Liquid-activated quantum emission from pristine hexagonal boron nitride for nanofluidic sensing. *Nature Materials* **22**, 1236-1242, doi:10.1038/s41563-023-01658-2 (2023).

45 Dean, J. A. *Lange's handbook of chemistry*. (1999).

46 Wakai, C., Oleinikova, A., Ott, M. & Weingärtner, H. How Polar Are Ionic Liquids? Determination of the Static Dielectric Constant of an Imidazolium-based Ionic Liquid by Microwave Dielectric Spectroscopy. *The Journal of Physical Chemistry B* **109**, 17028-17030, doi:10.1021/jp053946+ (2005).

47 Tomlin, R. J., Roy, T., Kirk, T. L., Marinescu, M. & Gillespie, D. Impedance response of ionic liquids in long slit pores. *Journal of The Electrochemical Society* **169**, 120513 (2022).

48 Sun, B. *et al.* Non–zero-crossing current-voltage hysteresis behavior in memristive system. *Materials Today Advances* **6**, 100056 (2020).

View Article Online
DOI: 10.1039/D5FD00142K

49 Brown, W. *et al.* Deconvolution of electroosmotic flow in hysteresis ion transport through single asymmetric nanopipettes. *Chemical Science* **11**, 5950-5958 (2020).

50 Brown, W., Kvetny, M., Yang, R. & Wang, G. Higher ion selectivity with lower energy usage promoted by electro-osmotic flow in the transport through conical nanopores. *The Journal of Physical Chemistry C* **125**, 3269-3276 (2021).

51 Bisquert, J., Roldán, J. B. & Miranda, E. Hysteresis in memristors produces conduction inductance and conduction capacitance effects. *Physical Chemistry Chemical Physics* **26**, 13804-13813 (2024).

52 Torriero, A. A. Understanding the differences between a quasi-reference electrode and a reference electrode. *Med. Anal. Chem. Int. J* **3**, 000144 (2019).

53 Cheng, L.-J. & Guo, L. J. Rectified ion transport through concentration gradient in homogeneous silica nanochannels. *Nano Letters* **7**, 3165-3171 (2007).

54 Gurina, D. & Budkov, Y. Understanding the role of confinement in the behavior of ionic liquid–organic solvent mixtures in slit carbon micropores: Insights from molecular dynamics. *Journal of Molecular Liquids* **419**, 126734 (2025).

55 He, X., Xiao, X., Guan, Y. & Cui, X. Ionic current rectification behaviors in quartz nanopipettes with ionic liquids/aqueous solution systems. *Electrochimica Acta* **528**, 146282, doi:https://doi.org/10.1016/j.electacta.2025.146282 (2025).

Data Availability Statement

View Article Online
DOI: 10.1039/D5FD00142K

Data supporting the findings of this study are available in Figshare at the following DOI: 10.6084/m9.figshare.30752456

All raw and processed datasets, analysis scripts, and supplementary figures used in this work have been deposited in accordance with the Royal Society of Chemistry data availability policy.